Available online at www.sciencedirect.com

ScienceDirect

Ceramics International 40 (2014) 2717–2722

CERAMICS INTERNATIONAL

www.elsevier.com/locate/ceramint

Sintering behavior and mechanical properties of alumina/zirconia multilayers composite via nano-powder processing

E. Salahi[a], H. Esfahani[a,*], I. Mobasherpour[a], M.A. Bijarchi[b], M. Taheri[c]

[a]Materials and Energy Research Center, PO Box 141554777, Tehran, Iran
[b]Tehran University, Faculty of Technology, Mechanical Department, Tehran, Iran
[c]Department of Materials Science and Engineering, McMaster University, Hamilton, Ontario, Canada L8S 4L7

Received 16 July 2013; received in revised form 12 October 2013; accepted 12 October 2013
Available online 22 October 2013

Abstract

The present research has been focused on the development of functionally graded alumina–zirconia composites, which particularly have high mechanical and thermal properties. In this study, different components of alumina–zirconia layers were enhanced between two layers of pure alumina and alumina with 20 mol% zirconia. The effect of this enhancement on consolidation, sintering condition, hardness and toughness values of the multilayer samples was evaluated. The results showed that the cracks were distributed in the co-sintering multi-layered structure. The cracks were formed due to the residual stress caused by differences in thermal expansion and sintering between successive layers. The final shape and mechanical properties of the gradual samples were found to be improved.

Keywords: C. Mechanical properties; Alumins; Multilayers; Zirconia

1. Introduction

The high strength, corrosion resistance, toughness and hardness of ZTA composites are the reason for their widespread application as advanced materials [1,2]. Functionally Graded Materials (FGM) are a group of the advanced materials characterized with gradient properties in three dimensions, in which the variations can be continuous or stepwise [3–5]. Reportedly, functionally graded, alumina–zirconia composites are well suited for structural applications due to their excellent contiguity behavior [6]. An examples of this is a fully dense, functionally graded alumina-ZTA with high mechanical properties produced by Rodriguez et al. [7]. Elsewhere, Novak et al. [8] prepared step-graded, ceramic composite samples including a ZTA core and an alumina surface with three to seven layers.

Various methods such as spark plasma sintering, slip casting, pulsed laser deposition, sedimentation particles, electrophoretic, powder processing and cathodic arc evaporation have been reported to fabricate FGM [9–15]. Among these, powder processing is widely used for fabricating multilayer materials due to its simple procedure [16]. Sun et al. [14] investigated many factors pertaining to fabricating crack-free, functionally graded, alumina–zirconia composites using powder processing. Nanoparticles of zirconia improve the fracture toughness of alumina matrix via micro-cracking, crack deflection, bridging and transformation toughening [17].

Overall, increasing the extent of t-ZrO_2in the body, will improve the fracture toughness of the composite [18,19]. However, the major obstacle to process the multi-layer materials is the crack propagation between the successive layers. Different thermal expansion coefficients (CTE) in the layers can induce compressive stresses at the interfaces [20]. Moreover, the different sinter ability of phases in FGM can lead to an increase in the particle spacing of nearly 2–30 μm [14].

*Corresponding author. Tel./fax: +98 26 3628 0040.
E-mail addresses: e-salahi@merc.ac.ir (E. Salahi), hap.esfahani@gmail.com, h-esfahani@merc.ac.ir (H. Esfahani), I-mobasherpour@merc.ac.ir (I. Mobasherpour), ali_bijarchi@ut.ac.ir (M.A. Bijarchi), taherm@mcmaster.ca (M. Taheri).

0272-8842/$ - see front matter © 2013 Elsevier Ltd and Techna Group S.r.l. All rights reserved.
http://dx.doi.org/10.1016/j.ceramint.2013.10.051

Al_2O_3 and ZrO_2 exhibit different thermal expansion coefficients (8.4×10^{-6}/°C vs. 10.3×10^{-6}/°C), and therefore, are susceptible to cracking during sintering. A solution for this is to increase the ZrO_2 at the interfaces to a considerable amount in order to control the crack propagation between the successive layers. Consequently, this study was carried out to better understand the role played by the median layers, with moderate ZrO_2 content, in the variation of bending, crack propagation, micro-hardness and fracture toughness of the sintered Al_2O_3/ZrO_2 multilayered composites.

2. Materials and methods

2.1. Powder preparation and consolidation

In order to obtain different layered structures, four sintered, bar, test samples (1 mm × 5 mm × 50 mm) were prepared. This provides A*x*Z test samples, in which A and Z represent Al_2O_3 and ZrO_2 respectively, whereas *x* represents the molar percentage of the ZrO_2. The mixed powders were prepared by adding reagent grades of α-Al_2O_3 as the composite matrix (27 nm with 99.5% purity), non-stabilized ZrO_2 as the second phase (30–60 nm with 99.9% purity) with 3 mol% Y_2O_3 as the tetragonal stabilizer (20–40 nm with 99.5% purity). The multi-layered structure was achieved by preparing the Al_2O_3 as the first step. Subsequently, an A20Z layer was added on top of the Al_2O_3 layer, and eventually the dual layer structure was consolidated using a cold uniaxial press with a 150 MPa load.

Similarly, samples nos. 3 and 4 with three and five successive layers were prepared, in accordance with the procedures described in Table 1. The sintering for all the samples was conducted at 1650 °C for 1 h with a heating rate of at 1650 °C for 1 h. The samples were then cooled down to the room temperature in the furnace with a cooling rate of 2.5 °C min^{-1}.

2.2. Sintering characterization

In order to measure the extent of bending occurred during the sintering, images were acquired from the cross-section of the samples. Wolfram Mathematica 8-2011 software was used to digitalize the images and a circle was fit on the bent edge of the samples in the X–Y plane. The radius of the fitted circle was then measured as a bending parameter. Subsequently, the percent of the bending was calculated via Eq. (1), in which B is the percent of bending, R_1 is the radius of the fitted circle for sample no. 1, and R_i is radius of the fitted circle for sample no. i (i=2, 3 and 4).

$$B = \frac{R_1 - R_i}{R_1} \times 100 \quad (1)$$

Table 1
Codes and number of layers in each sample.

Sample code	Number of layers	Layers of composite
1	1	A
2	2	A/A20Z
3	3	A/A10Z/A20Z
4	5	A/A5Z/A10Z/A15Z/A20Z

2.3. Phase and microstructure analyze

The crystallographic composition of A20Z, adjacent to the outer layer, was analyzed using an X-ray diffractometer (Philips Model PW2773) with a Ni filtered Cu-kα radiation. In addition, the cross-sections of the samples was examined using a SEM platform (Vega\\TScan-20 kV) equipped with EDS (Oxford Inca with a silicon (Si) drift detector) operated at accelerating voltages of 30 kV. SEM images were used to elucidate the crack propagation and the microstructures of the interface, whereas the EDS results indicated the distribution of zirconium atoms in the matrix.

2.4. Microhardness and fracture toughness measurements

The cross-section coupons were mechanically polished with napless paper using a H_2O-based diamond suspensions of 3 μm and 1 μm. Vickers hardness (HV) tests were conducted on the as-polished samples in accordance with ASTM E384-11E1 using a 500 g force and the fracture toughness (K_{IC}) values were calculated. To ensure the reproducibility, the set of measurements were repeated for four times and the average values were reported.

Eq. (2) was used to calculate the fracture toughness values [21], in which D is the corner crack length measured from the center of the indent in (mm), P is the indentation load (kgf), E is Young's modulus (GPa) and H is the hardness (GPa). Young's modulus was calculated using the simple mixture rule of composites [22].

$$K_{1C} = 0.016\left(\frac{E}{H}\right)^{1/2}\left(\frac{P}{D^{3/2}}\right) \quad (2)$$

3. Results and discussion

The differences between the coefficients of thermal expansion (CTE) in successive layers is the main reason for induction of interfacial stresses. Moreover, variations in densification or composition of the layers can also create residual stresses [23,24].

Fig. 1 shows the deformation of prepared samples after sintering. The multi-layer samples are bent in form of a semicircle in the X–Y plane, whereas the bending in the *z* direction is negligible. Different shrinkage strain, present at the interface of the layers, led to the bending of the samples. This indicates that the thermal strain is a result of different CTE. Sample no. 2 exhibits the maximum percent of bending due to the greatest compositional difference between the adjacent layers. The percent of bending is decreased by modifying sample no. 2 from the opposition structure to the gradient structure. The results indicated that the percent of bending of sample no. 3 decreased from 99.81% to 99.76%, once the A10Z middle layer was enhanced at the interface. The percent

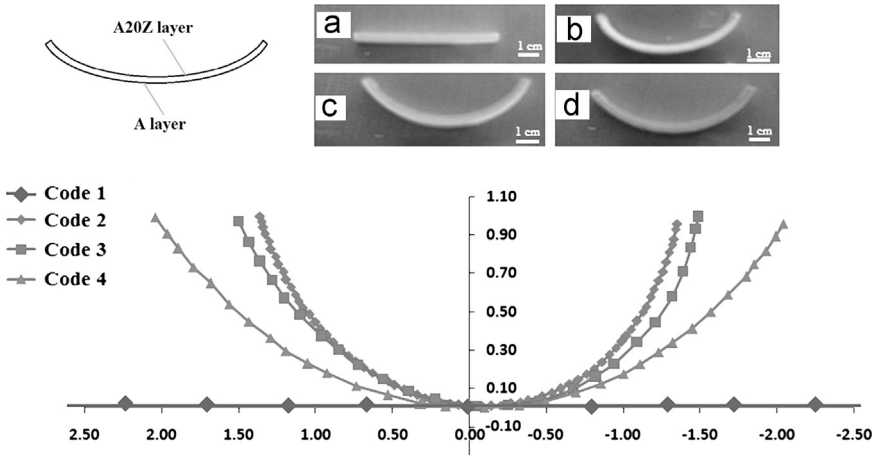

Fig. 1. Cross view of deformed samples after sintering (a) Code 1, (b) Code 2, (c) Code 3 and (d) Code 4.

of bending in sample 4 was measured 99.65%. Therefore, enhancements of A5Z and A15Z layers improved the bending resistance. Consequently, enhancement of the middle layer, coordinates the differences between the CTEs of the outer layers, and therefore, reduces the residual stress.

Fig. 2 shows the distribution of ZrO_2 in sample no. 4. The BSE–SEM image acquired from sample 4 is shown in Fig. 2a. In the back scatter electron (BSE) mode, the gray spots indicate Al_2O_3, whereas the white spots indicate the ZrO_2 particle due to their different BSE coefficients. The EDS spectra acquired from this area confirmed that the white spots belonged to zirconium (Fig. 2b). The elemental X-ray EDS maps of aluminum and zirconium, shown in Fig. 2c and d, confirm the formation of a gradient structure. Five adjacent layers are also evident, as depicted by the distribution of zirconium. These results suggest that the mechanical properties including hardness and fracture toughness vary through the gradient structure.

The X-ray diffraction pattern of α-Al_2O_3 content of 20 mol% ZrO_2 is shown in Fig. 3. Three pairs of peaks, found at diffraction angles of 35°, 50° and 59°, are attributed to the tetragonal phase, whereas two weak peaks sat 2θ of 30° correspond to the monoclinic phase [18]. In addition, no extra peak corresponding to a foreign phase was identified in the XRD pattern. The fraction of tetragonal ZrO_2 was calculated using the Gravie and Nicholson method [25] (Eq. (3)), in which I_t and I_m represent the integrated intensity of the tetragonal (101) and monoclinic (111), $(\bar{1}11)$ peaks respectively. According to the XRD results, the fraction of the stabilized tetragonal phase at the room temperature was estimated about 0.95. This indicates that the stabilizing process has been completely performed. Therefore, a ZrO_2 containing layer is likely formed and has improved the mechanical properties.

$$X_t = 1 - \frac{I_m(11\bar{1}) + I_m(111)}{I_m(11\bar{1}) + I_m(111) + I_t(101)} \quad (3)$$

In a previous study, the authors reported that the remained monoclinic phase increases with the increase of ZrO_2 content in the Al_2O_3–ZrO_2 composites with a similar sintering condition [26]. Therefore, it suggests that the middle layers with lower amount of ZrO_2 exhibit higher tetragonal fraction. Moreover, the middle layers will be able to promote the transformation toughening as well as the A20Z layer.

According to the rule of composites, the CTE will decrease by increasing the ZrO_2 content [22]. The differences in the shrinkage rates of the adjacent layers during the final step of the sintering create tensile and compressive stresses at the interface. The results showed that the layer with the higher ZrO_2 content is more consolidated. Therefore, compressive stresses are induced on its surface and the tensile stresses remained on the next layer. The initiated cracks can now propagate in the layers experiencing tensile stresses, located in between the layers under compression. The presence of cracks in the Al_2O_3 layers confirm that they have been propagated under tensile stresses. In contrast, no cracks were propagated in ZrO_2 containing layers (see Fig. 4).

Micro-hardness of each layer was measured at three different points and the average values are plotted against the distance from the outer surface of Al_2O_3, as shown in Fig. 5a–c. The results indicate that the hardness of the layers in all samples is decreased by increasing the ZrO_2 content due to the lower hardness of ZrO_2 versus Al_2O_3. In addition, the Vickers hardness depends on the size and extents of the porosity [27]. Fig. 6 shows the interface of A and A20Z layers in sample 2. The differences in the heat properties of A and A20Z have likely compromised the condition of sintering final step. Therefore, evidently, different amounts of surface porosity are found to be formed on A and A20Z layers.

The hardness of A and A20Z layers was found to be increased with the change in the structure of the sample by increasing the extent of the ZrO_2 containing layer (Fig. 5b and c). This behavior can be elucidated by the moderation of heat properties of layers. The AxZ (x=5, 10 and 15) layer decreased the differences of CTE and also improved the sintering conditions. Therefore, in functionally graded sample, the percent of bending and the final porosity formed by sintering are decreased to the minimum value. The hardness of A and A20Z layers are also increased. The maximum hardness of A and A20Z layers are achieved in sample no. 4.

Fracture toughness of each layer was calculated based on Eq. (2) and the results are plotted against the distance from the

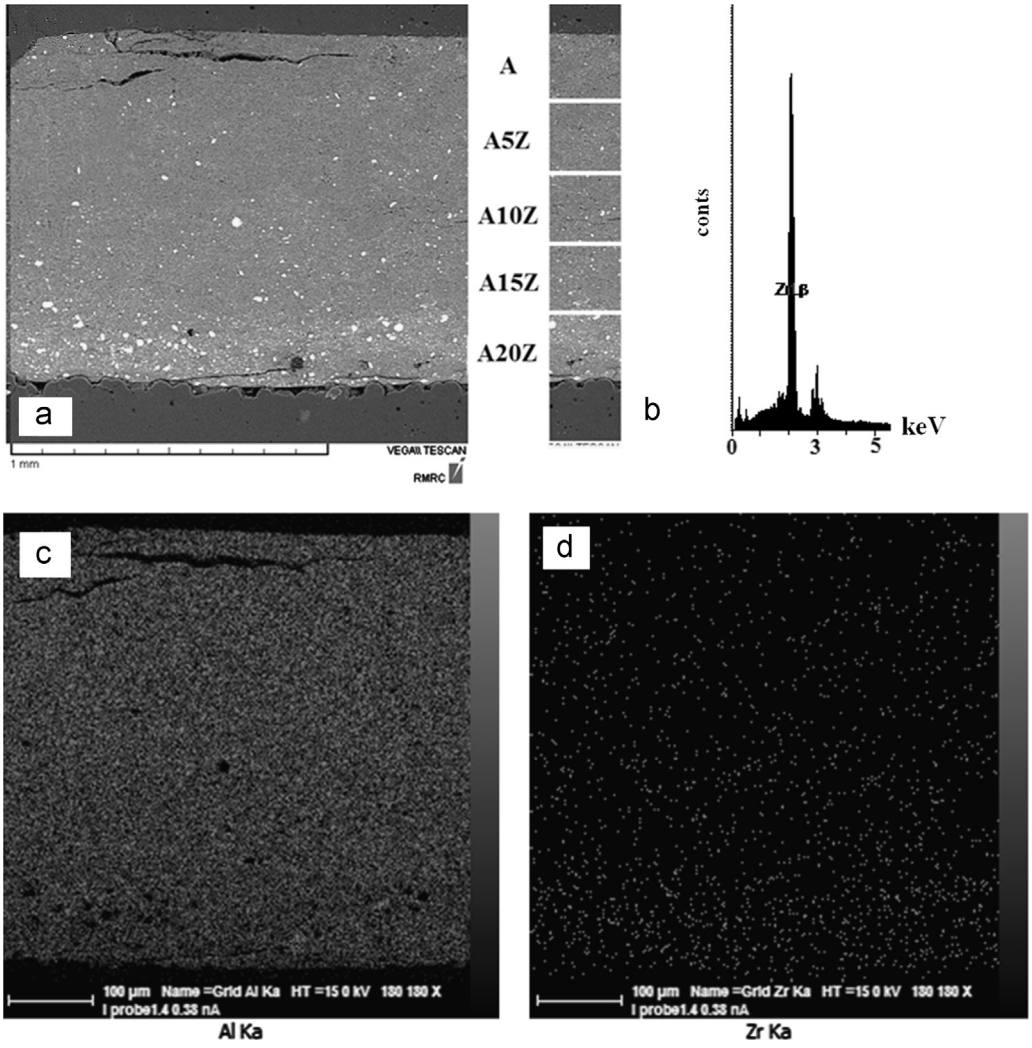

Fig. 2. (a) BS-SEM cross image of sample 4, (b) EDS of one white spot from Fig. 2a, (c) Al and (d) Zr X-ray map of Fig. 2a.

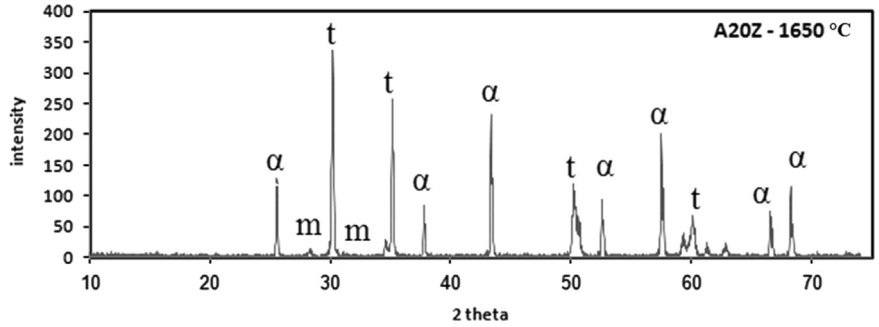

Fig. 3. X-ray diffraction pattern of A20Z layer sintered at 1650 °C.

outer surface of alumina, as shown in Fig. 5d–f. Although hardness and Young's modulus of ZrO_2 layers are declined, the *E*/*H* ratio of the ZrO_2 layers increased by increasing the ZrO_2 content. The calculated *E*/*H* ratios for A5Z, A10Z, A15Z and A20Z were 24.63, 28.95, 31.83 and 33.77 respectively. Therefore, it is expected that the fracture toughness of the layers increase by increasing the ZrO_2 content. The measured fracture toughness of sample no. 4, shown in Fig. 5f, indicates that the fracture toughness of the layers is increased by increasing the ZrO_2 content. Interestingly, not only the increase of *E*/*H* parameter resulted in improving the fracture toughness, but also the decrease of the crack parameter (*D*) led to increasing the fracture toughness of the ZrO_2 containing layers. The measured crack parameters have been shown in Table 2. The results indicated that the calculated crack parameters of A and A20Z layer decreased from 47.31 µm

and 32.56 μm in sample 2 to 43.89 μm and 29.42 μm in sample 4 respectively. Crack bridging, micro-cracks and transformation toughening could be activated together or separately in sintered ZrO_2ceramics and decrease the crack parameter [18]. Although the fraction of the tetragonal phase was decreased by increasing the ZrO_2 content, the potential of the sites for activating one mechanism of toughening was increased. Increasing the second phase in Al_2O_3 matrix, multiplied the number of toughened sites and the ZrO_2 particles became more uniformly. The results showed that in the layers with more ZrO_2 content, the crack parameter (D) is lower than that measured in the layers with less ZrO_2 content. Therefore, a toughening mechanism has likely dominated and the fracture toughness was then improved.

Fracture toughness of A and A20Z layers were increased via modifying the dual-layer structure to a multi-layer structure. Furthermore, the graded thermal properties led to moderate sintering conditions and increased the shrinkage of the outer layers. Therefore, the open surface porosities declined and the fracture toughness increased.

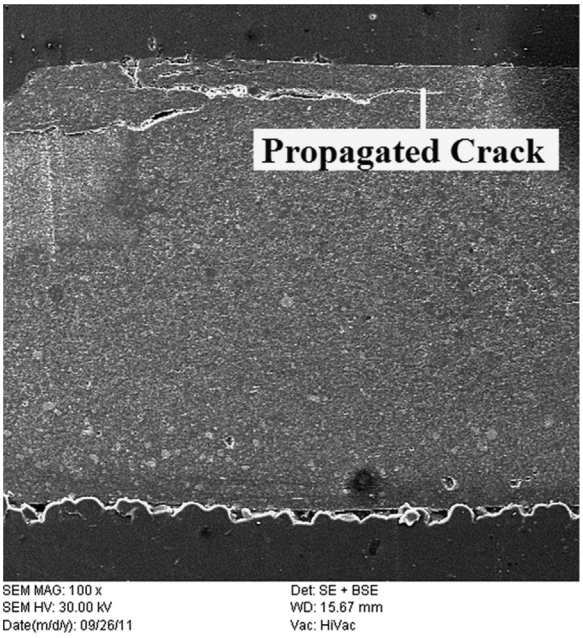

Fig. 4. SEM cross image of sample 4, crack propagated in alumina layer (remind tensile stress) and no cracks propagated in zirconia layers.

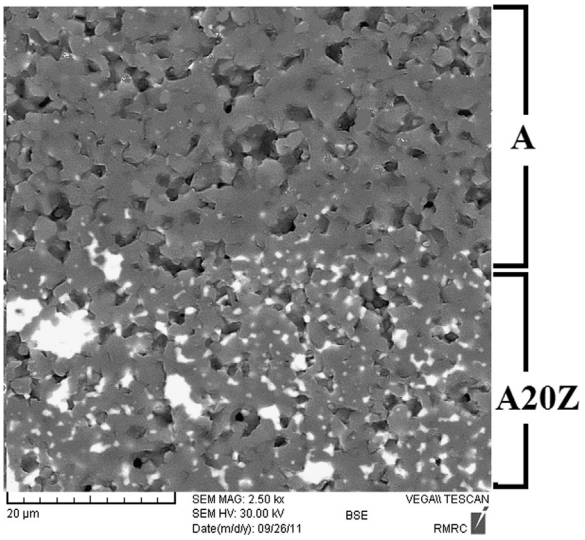

Fig. 6. The BS-SEM image for interface of A and A20Z layers in sample 2.

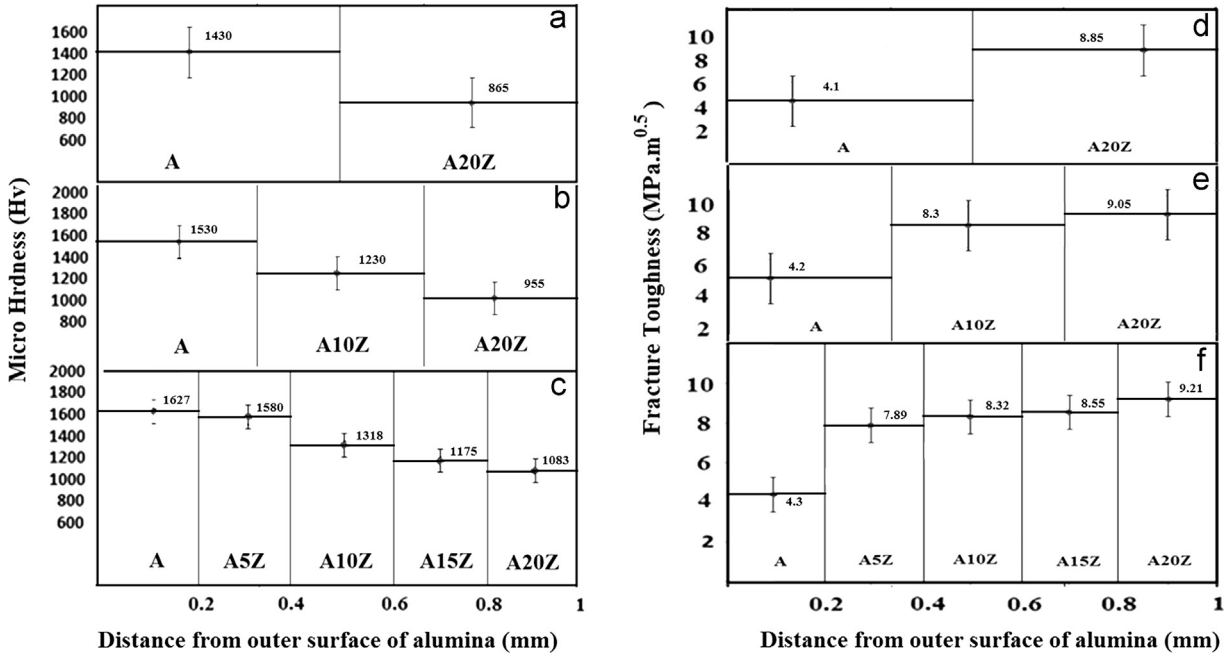

Fig. 5. Variations of hardness and fracture toughness amount versus distance from alumina surface: (a,d) sample 2, (b,e) sample 3 and (d,f) sample 4.

Table 2
Measured crack parameters.

Layers	D (μm)		
	Sample 2	Sample 3	Sample 4
A	47.31	45.52	43.89
A5Z	–	–	29.36
A105Z	–	30.67	29.91
A15Z	–	–	30.32
A20Z	32.56	31.04	29.42

4. Conclusion

In order to investigate the mechanical properties of multi-layered Al_2O_3–ZrO_2 composites, dual, triple and quintuple layer samples with different compositions were fabricated via the powder processing technique. Differences in the compositions and the number of the layers resulted in different final shapes. Changing the dual-layer structure to a multi-layer structure decreased the bending due to minimizing the differences of thermal properties. Change the thermal expansion coefficient (CTE) in multi-layer sample affected the densification and mechanical properties. The results also showed that the hardness and fracture toughness values of the multi-layer structure were higher than the double-layer structure. In multi-layer samples the hardness decreased, whereas the fracture toughness increased by increasing the ZrO_2 content. In addition, the X-ray diffraction pattern of the sintered A20Z layer indicated that 95% of ZrO_2 particles were formed as tetragonal phase.

References

[1] K. Tahmasebi, M.H. Paydar, The effect of starch addition on solution combustion synthesis of Al_2O_3–ZrO_2 nanocomposite powder using urea as fuel, Mater. Chem. Phys. 109 (2008) 156–163.

[2] G. de Portu, L. Micele, G. Pezzotti, Laminated ceramic structures from oxide systems, Compos. Part B 37 (2006) 556–567.

[3] N. Chopra, Multifunctional and multi component hetero structured one-dimensional nanostructures: advances in growth, characterization, and applications, Mater. Sci Technol.: Adv. Perform. Mater. 25 (2010) 212–230.

[4] D.C. Pender, S.C. Thompson, N.P. Padture, A.E. Giannakopoulos, S. Suresh, Gradients in elastic modulus for improved contact-damage resistance. Part ii: the silicon nitride–silicon carbide system, Acta Mater. 49 (2001) 3263–3268.

[5] Q.D. Qin, Y.G. Zhao, P.J. Cong, Y.H. Liang, W. Zhou, Functionally graded Mg_2Si/Al composite produced by an electric arc remelting process, J. Alloys Compd. 420 (2006) 121–125.

[6] E.M.M. Ewais, D.H.A. Besisa, Z.I. Zaki, A.E.H.T. Kandil, Tailoring of functionally graded zirconia–mullite/alumina ceramics, J. Eur. Ceram. Soc. 32 (8) (2012) 1561–1573.

[7] A. Morales-Rodriguez, A. Dominguez-Rodriguez, G. de Portu, M. Jimenez-Melendo, Creep mechanisms of laminated alumina/zirconia-toughened alumina composites, J. Eur. Ceram. Soc. 29 (2009) 1625–1630.

[8] S. Novak, M. Kalin, P. Lukas, G. Anned, J. Vleugels, O. Van Der Biest, The effect of residual stresses in functionally graded alumina–ZTA composites on their wear and friction behavior, J. Eur. Ceram. Soc. 27 (2007) 151–156.

[9] W. Jiang, J.F. Zhang, L.J. Wang, R. Tu, X.Q. Yang, G. Chen, P.C. Zhai, Ti_3SiC_2–(Ti_3SiC_2–SiC) functionally graded materials by spark plasma sintering reactive synthesis method Part 2 – fabrication and characterization, Mater Techol. Adv. Perform. Mater. 25 (2010) 283–288.

[10] L. Heidy, C. Pulgarin, L.B. Garrido, P. Albano, Processing of different alumina–zirconia composites by slip casting, Ceram. Int. 39 (6) (2013) 6657–6667.

[11] P.H. Tang, R.G. Song, G.Z. Chai, J. Mao, Microstructure and nano indentation hardness of TiN/AlN multilayer films prepared by pulsed laser deposition, Surf. Eng. 28 (2012) 165–170.

[12] Ch. Fei, Yu. Lichun, Sh. Qiangand, Zh. Lianmeng, Fabrication of TZ-3Y20A/Mo multilayer composites by particle sedimentation method, J. Mater. Process Technol. 199 (2008) 37–40.

[13] X. Wang, E.A. Olevsky, E. Bruce, M.B. Stern, D.T. Hayhurst, Fabrication of functionally graded 3A/5A zeolites by electrophoretic deposition, Surf. Eng. 23 (2007) 443–447.

[14] L. Sun, A. Sneller, P. Kwon, Fabrication of alumina/zirconia functionally graded material: from optimization of processing parameters to phenomenological constitutive models, Mater. Sci. Eng. A 488 (2008) 31–38.

[15] B. Warcholinski, A. Gilewicz, Mechanical properties of multilayer TiAlN/CrN coatings deposited by cathodic arc evaporation, Surf. Eng. 27 (2011) 491–497.

[16] B. Kieback, A. Neubrand, H. Riedel, Processing techniques for functionally graded materials, Mater. Sci. Eng. A 362 (2003) 81–105.

[17] F. Cesari, L. Esposito, F.M. Furgiuele, C. Maletta, A. Tucci, Fracture toughness of alumina–zirconia composites, Cram. Int. 32 (3) (2006) 249–255.

[18] S.S. Zhang, S.O. Chen, D. Li, W.Q. Shao, H.S. Cao, Phase analysis of Al_2O_3–ZrO_2 composite powders prepared by co-precipitation method, Mater. Technol. Adv. Perform. Mater. 23 (2008) 220–223.

[19] F. Kern, P. Palmero, Microstructure and mechanical properties of alumina 5 vol% zirconia nano composites prepared by powder coating and powder mixing routes, Ceram. Int. 39 (1) (2013) 673–682.

[20] P. Hvizdos, D. Jonsson, M. Anglada, G. Anne, O.V.D. Biest, Mechanical properties and thermal shock behaviour of an alumina/zirconia functionally graded material prepared by electrophoretic deposition, J. Eur. Ceram. Soc. 27 (2–3) (2007) 1365–1371.

[21] G.R. Anstis, P. Chantikul, B.R. Lawn, D.B. Marshall, A critical evaluation of indentation techniques for measuring fracture toughness. I. Direct crack measurements, J. Am. Ceram. Soc. 64 (1981) 533–538.

[22] S. Muraishi, Mixture rule for indentation derived Young's modulus in layered composites, Thin Solid Films 518 (1) (2009) 233–246.

[23] E. Stoll, P. Mahr, H.-G. Kruger, H. Kerna, B.J.C. Thomasb, A.R. Boccaccini, Fabrication technologies for oxide–oxide ceramic matrix compositesbased on electrophoretic deposition, J. Eur. Ceram. Soc. 26 (2006) 1567–1576.

[24] W.Q. Shao, S.O. Chen, H.S. Cao, D. Li, Y.C. Zhang, S.S. Zhang, Relationship of densification rate and relative density for submicron α-Al_2O_3 green compacts during low heating rate sintering, Mater. Technol. Adv. Perform. Mater. 23 (2008) 148–151.

[25] R.C. Garvie, P.S. Nicholson, Phase analysis in zirconia systems, J. Am. Ceram. Soc. 5 (1972) 303–305.

[26] H. Esfahani, A. Nemati, E. Salahi, Adv. Mater. Res. 93-94 (2010) 695–698.

[27] J.M. Tulliani, C. Bartuli, E. Bemporad, V. Naglieri, M. Sebastiani, Preparation and mechanical characterization of dense and porous zirconia produced by gel casting with gelatin as a gelling agent, Ceram. Int. 35 (6) (2009) 2481–2491.